Exciton wave function localization and exciton diamagnetic coefficient in semiconductor quantum rings without reflection symmetry

Oleksandr Voskoboynikov,[1,*] W. T. Chiu,[1] and L. M. Thu[1,2]

[1]*Department of Electronic Engineering and Institute of Electronics, National Chiao Tung University, 1001 Ta Hsueh Road, Hsinchu 300, Taiwan, Republic of China*

[2]*Department of Physics, Hanoi National University of Education, 136 Xuanthuy Road, Hanoi, Vietnam*

(Received 19 June 2013; published 12 August 2013)

We theoretically study how reflection asymmetry affects the neutral exciton diamagnetic coefficient in self-assembled InGaAs/GaAs semiconductor wobbled quantum rings. The previously proposed mapping method is used to simulate the exciton wave function and energy in the rings. The description is suited to clarify the important question of the exciton diamagnetic coefficient stability in the rings with broken reflection symmetry. Our simulation results confirm that the exciton wave function of the reflection symmetrical (balanced) wobbled ring is distributed equally over two potential valleys corresponding to the hills in the ring's shape. At the same time, even a very small reflectional imbalance in the geometry and (or) material content of the wobbled rings destroys the ringlike shape of the exciton wave function and causes the localization of the function in one of the potential valleys of the ring (dotlike shape of the exciton wave function). This leads to a rapid decrease of the exciton diamagnetic coefficient. Our calculation results are in good agreement with recent experimental observations.

DOI: 10.1103/PhysRevB.88.085310 PACS number(s): 73.21.La, 78.67.Hc

I. INTRODUCTION

Semiconductor self-assembled quantum rings (SAQRs) are nano-objects of a non-simply-connected topology.[1–5] This distinctive characteristic of SAQRs recently has attracted considerable attention. It is assumed that SAQR specific geometry and the absence of crystal defects and impurities can provide experimentalists with the unique opportunity to observe topological quantum effects for charged particles confined in the SAQRs (including the optical Aharonov-Bohm effect).[6–15] Impressive progress in semiconductor nanofabrication technology makes it possible to produce and investigate SAQRs within a wide range of geometrical and material parameters (see, e.g., Refs. 16–28 and references therein). Among them, $In_cAs_{1-c}Ga/GaAs$ SAQRs have been investigated extensively both experimentally and theoretically (see, for instance, Refs. 3, 8, 11, 13–15, 17, 26, and 28–43). It was found that magnetic and magneto-optical properties of the rings strongly depend on their actual geometrical and material parameters. At the same time, the shape of embedded $In_cAs_{1-c}Ga/GaAs$ SAQRs grown on a (001) surface of a GaAs substrate in general does not possess cylindrical symmetry. The height of the $In_cAs_{1-c}Ga/GaAs$ ring at the rim (and In concentration near the rim) is larger along the [110] direction (x axis in Fig. 1) than in the $[1\bar{1}0]$ direction (y axis in Fig. 1).[17,34] This forms two distinct hills in the ring's shape (and correspondingly two potential valleys for electrons and holes) along the x direction (see Fig. 1). The "wobbled" geometry affects the magnitude of the single-electron magnetization oscillation[35,36,43] and exciton diamagnetic response[13,37–39] of the rings.

The ground-state energy of an exciton in a weak magnetic field (B) can be presented by

$$E_{\rm ext}(B) = E^0_{\rm ext} + s\mu_B g_{\rm ext} B + \alpha_d B^2,$$

where $E^0_{\rm ext}$ stands for the exciton energy at $B = 0$ T, μ_B is the Bohr magneton, $g_{\rm ext}$ is the exciton Landé factor, $s = \pm 1$ presents the exciton spin polarization along the magnetic field direction, and α_d is the exciton diamagnetic coefficient. The diamagnetic coefficient is obviously connected to the second derivative of the exciton energy with respect to the magnetic field magnitude and for the weak-field limit: $\alpha_d = \frac{1}{2}\frac{d^2E_{\rm ext}}{dB^2}|_{B=0}$.[15,40] In the strong confinement regime[10,41] (when the magnetic field is applied along the system growth direction, z axis), the coefficient can be evaluated by using the effective radii (the characteristic confinement lengths) of the electron ρ_e and hole ρ_h in the plane perpendicular to the magnetic field,[44]

$$\alpha_d = \frac{e^2}{8}\left(\frac{\rho_e^2}{m_e} + \frac{\rho_h^2}{m_h}\right),$$

where e is the electronic charge and $m_{e(h)}$ stands for the electron (hole) effective mass. Therefore, the actual value of the exciton diamagnetic coefficient can be used for a preliminary estimation of the exciton confinement length. In some recent experiments[13,38] (and earlier),[8] it has been found that for some asymmetrical SAQRs, the diamagnetic coefficient for neutral excitons can be surprisingly small (considerably smaller than that expected from the conventional theory). In Ref. 38, it was proposed that the lack of the perfect rotation symmetry (for wobbled rings) is a reason for the hole localization in one of the potential valleys of the rings (which corresponds to one of the hills in the rings shape). Due to the electron-hole Coulomb interaction, the hole's localization should lead to a localized exciton wave function (in the same potential valley), which decreases the neutral exciton effective confinement length and diamagnetic coefficient. However, the geometrical model of the wobbled ring in Ref. 38 still possesses the reflection symmetry with respect to the reflection in the y-z plane. According to a general symmetrical consideration, the ground-state wave functions

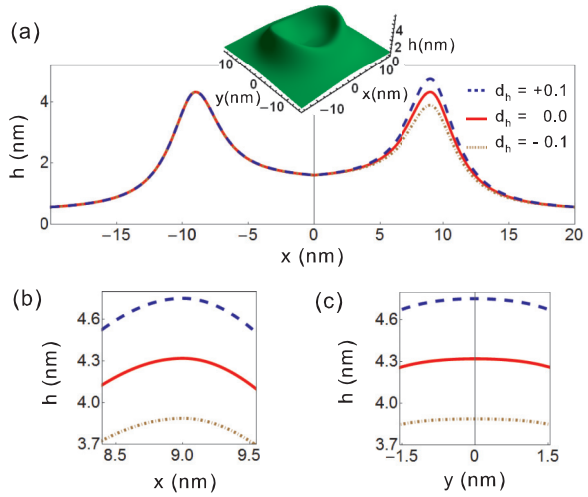

FIG. 1. (Color online) Cross section of the ring structure for different values of the parameter d_h and $x_p = R(1+\xi_R)$: (a) Cross section by the (x,y_p,z) plane (inset: general shape of the $In_cGa_{1-c}As/GaAs$ wobbled SAQR); (b) zoom of the cross section by the (x,y_p,z) plane near $x = x_p$; (c) cross section by the (x_p,y,z) plane. Remark: type-*A* ring is presented; see descriptions below and Table. I.

of the electron and hole confined in the ring consequently should possess the same reflection symmetry.[45] The symmetry cannot be broken by the electron-hole Coulomb interaction in a dielectric structure of the same reflection symmetry. Therefore, the ground-state exciton wave function has to be distributed symmetrically between two symmetrical potential valleys. This fact raises the question about the actual reason for the decrease of the neutral exciton confinement length and diamagnetic coefficient in the wobbled rings.

In this paper, we theoretically study the impact of the broken reflection symmetry on the diamagnetic coefficient of the ground state of the neutral exciton confined in $In_cAs_{1-c}Ga/GaAs$ SAQRs. Using our mapping method,[43,46] we can efficiently reproduce three-dimensional geometrical shapes and material compositions of the rings and simulate excitonic properties of the rings with the reflection symmetry and when the symmetry is broken. We demonstrate that for the rings with reflection symmetry with respect to reflection in the (110) plane (y-z plane in Fig. 1), the ground-state exciton wave function is equally distributed (balanced) between two potential valleys of the rings. But, a small imbalance in geometrical or material characteristics of the rings along the [110] direction (x axis in Fig. 1) leads to the localization of the exciton wave function in one of the potential valleys of the ring, which causes a significant decrease of the exciton diamagnetic coefficient.

II. THEORETICAL MODEL

To simulate $In_cAs_{1-c}Ga/GaAs$ wobbled SAQRs with and without the reflection symmetry, we adopt the model of the ring's height profile from Ref. 36 with some modifications. This model suggests that the bottom of the ring is perfectly flat and parallel to the x-y plane. The height of the ring $h(x,y)$ along the z direction (Fig. 1) can be written as follows:[36,43]

$$\begin{aligned} h(x,y) &= h_0 + \frac{[\widetilde{h}_M(x,y)-h_0]\widetilde{\gamma}_0(x,y)^2}{\Delta R(x,y)^2+\widetilde{\gamma}_0(x,y)^2} \\ &\quad\times \frac{\widetilde{R}(x,y)^2-\Delta R(x,y)^2}{\widetilde{R}(x,y)^2}, \ \sqrt{x^2+y^2} \leqslant \widetilde{R}(x,y), \\ h(x,y) &= h_\infty + \frac{[\widetilde{h}_M(x,y)-h_\infty]\widetilde{\gamma}_\infty(x,y)^2}{\Delta R(x,y)^2+\widetilde{\gamma}_\infty(x,y)^2}, \ \sqrt{x^2+y^2} > \widetilde{R}(x,y), \end{aligned} \tag{1}$$

with

$$\widetilde{h}_M(x,y) = h_M\left(1+\xi_h\frac{x^2-y^2}{x^2+y^2}\right)F_h(x,y), \tag{2}$$

$$\widetilde{R}(x,y) = R\left(1+\xi_R\frac{x^2-y^2}{x^2+y^2}\right), \tag{3}$$

$$\Delta R(x,y) = \sqrt{x^2+y^2}-\widetilde{R}(x,y), \tag{4}$$

$$\widetilde{\gamma}_0(x,y) = \gamma_0\left(1+\xi_\gamma\frac{x^2-y^2}{x^2+y^2}\right), \tag{5}$$

$$\widetilde{\gamma}_\infty(x,y) = \gamma_\infty\left(1+\xi_\gamma\frac{x^2-y^2}{x^2+y^2}\right), \tag{6}$$

$$F_h(x,y) = 1+d_h\exp\left[-\frac{(x-x_p)^2+(y-y_p)^2}{b^2}\right], \tag{7}$$

where R is the ring's rim average radius; h_0, h_r, and h_∞, respectively, stand for the height at the center of the ring, at the rim, and far outside of the ring; γ_0 and γ_∞, respectively, determine the inside and outside slopes near the ring's rim. The wobbling parameters ξ_h, ξ_R, and ξ_γ describe the anisotropy (circular asymmetry) of the ring height on the x-y plane. The reflection asymmetry in the ring hills' heights (the ring shape's reflection asymmetry) is described by the function $F_h(x,y)$, where $\{x_p = \pm R(1+\xi_R), y_p = 0\}$ stands for the position of the appropriate ring's profile maximum (top of the ring's hills; see Fig. 1), and the range of the reflection asymmetry in the wobbling is presented by a parameter b. According to Eq. (1), in our model deviations from the reflection symmetry in the ring's shape are controlled by a unitless parameter d_h as

$$d_h = \frac{h(x_p,y_p)|_{d_h\neq 0}-h(x_p,y_p)|_{d_h=0}}{h(x_p,y_p)|_{d_h=0}}. \tag{8}$$

In Fig. 1, we present the shape of the structure and cross sections of the ring by (x,y_p,z) and (x_p,y,z) planes for different d_h when the ring height deviations are concentrated at the position of the maximum at the positive $x_p = R(1+\xi_R)$ and $y_p = 0$.

We use $h(x,y)$ to describe the corresponding three-dimensional smooth confinement potential for electrons (holes) by the shape and composition-dependent profiles of the local conduction (e) and valence (h) band offsets:[43,46]

$$V_{e(h)}(\mathbf{r}) = \Delta E^0_{e(h)}[1-F_V(\mathbf{r})T(\mathbf{r})], \tag{9}$$

where

$$T(\mathbf{r}) = \frac{1}{4}\left[1+\tanh\left(\frac{z}{a}\right)\right]\left\{1-\tanh\left[\frac{z-h(x,y)}{a}\right]\right\}, \quad (10)$$

$$F_V(\mathbf{r}) = 1 + d_V\left\{\exp\left[-\frac{(x-x_p)^2+(y-y_p)^2}{b^2}\right] \times \exp\left[-\frac{(z-z_p)^2}{b_z^2}\right]\right\}. \quad (11)$$

$\mathbf{r} = (x,y,z)$ is the three-dimensional radius vector, $\Delta E^0_{e(h)} = E^{\text{out}}_{c(v)} - E^{\text{in}}_{c(v)}$ is the overall conduction (valence) band offset between the inner and outer semiconductor materials in the InGaAs/GaAs heterostructure, and superscripts "in" and "out" denote the actual material parameters inside and outside the ring. The slope and range (the degree of smoothness) of the potential change at the boundaries of the ring are controlled by a parameter a [when the parameter a goes to 0, Eq. (9) describes a rigorous full three-dimensional hard-wall potential]. In addition to the ring's shape asymmetry (controlled by d_h), the reflection asymmetry in the ring's potential (the reflection asymmetry in the ring's material content) is presented by the function $F_V(\mathbf{r})$, where $\mathbf{r}_p = (x_p, y_p, z_p)$ refers to the position of the appropriate potential valley, and the range of the asymmetry in the z direction is presented by a parameter b_z. Deviations from the reflection symmetry in the ring's potential are controlled by a unitless parameter d_V, which, according to Eq. (9), can be presented as

$$d_V = \frac{V_{e(h)}(\mathbf{r}_p)|_{d_V=0} - V_{e(h)}(\mathbf{r}_p)|_{d_V\neq 0}}{\Delta E^0_{e(h)}} + O\left(\frac{a}{z_p}\right). \quad (12)$$

This approximate relationship becomes exact when $a \to 0$. Following the actual three-dimensional shape and content of the ring, Eq. (9) represents the three-dimensional confinement potential for electrons (holes) with the smooth changes of the material parameters across the boundaries of the ring.[46] Deviations of the parameter d_V obviously mimic the material content deviations at the hill locations of the wobbled ring. The local band offsets for electrons and holes grow when d_V is positive and increases. The offsets locally decrease when d_V is negative and its absolute value increases. In Figs. 2 and 3, we demonstrate some projections of the asymmetrical confinement potential defined by Eq. (9).

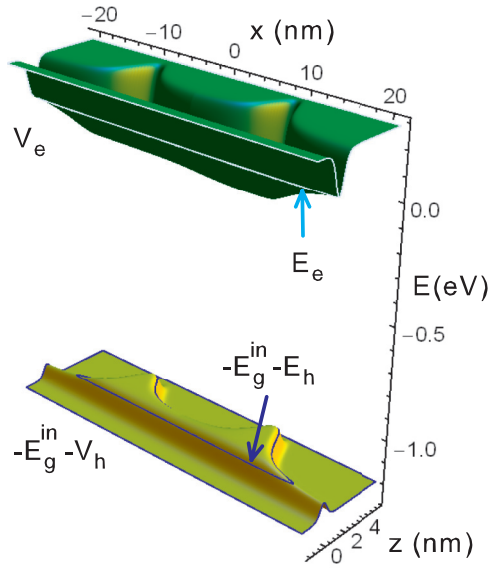

FIG. 2. (Color online) Projections of the electron (V_e) and hole ($-V_h$) confinement potentials (with the actual energy gap in between) on the (x,y_p,z) plane [$d_h = d_V = 0.1$ and $x_p = R(1+\xi_R)$]. E_e and $-E^g_{\text{in}} - E_h$ denote the electron and hole ground-state energies. Remark: type-A ring is presented; see descriptions below and Table I.

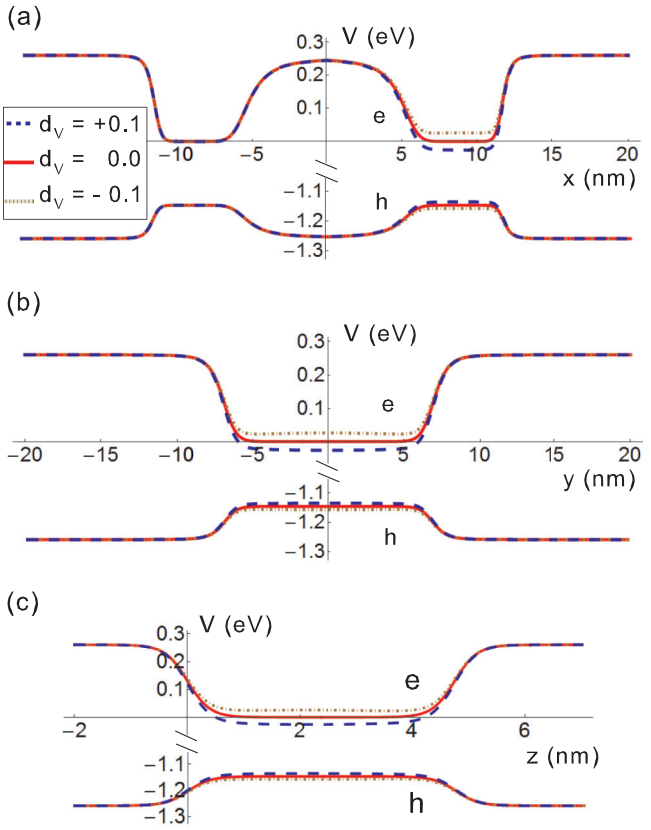

FIG. 3. (Color online) Electron ($e \Leftrightarrow V_e$) and hole ($h \Leftrightarrow -E^g_{\text{in}} - V_h$) confinement potential profile along different directions in the ring and for different values of the parameter d_V [$d_h = 0.1$ and $x_p = R(1+\xi_R)$]: (a) $[x,y_p,z_p]$ direction; (b) $[x_p,y,z_p]$ direction; (c) $[x_p,y_p,z]$ direction. Remark: Type-A ring is presented; see descriptions below and Table. I.

According to the available experimental data, two parameters d_h and d_V can be correlated: the height of a wobbled ring at the rim reflects the profile of the actual In concentration in the ring.[17,34] However, it is very difficult to derive this correlation. Therefore, to make this theoretical study more self-contained, we consider independently and cumulatively the impacts of the ring's shape reflection asymmetry and content reflection asymmetry on the exciton diamagnetic coefficient. When the parameters have the same sing, we can consider their changes as "correlated." When the signs are opposite, the parameters' changes can be considered as "anticorrelated."

Using $V_{e(h)}(\mathbf{r})$, we define the mapping function $M_{e(h)}(\mathbf{r})$ for electrons (holes) which accumulates experimental information about the ring's shape and local material content[43,46] as

follows:

$$M_{e\,(h)}(\mathbf{r}) = 1 - \frac{V_{e\,(h)}(\mathbf{r})}{\Delta E_{e\,(h)}}. \tag{13}$$

According to Eq. (13), the mapping functions for electrons and holes can be different only when $F_V(\mathbf{r})$ is different for these particles. An appropriate modification obviously requires extra parameters to be introduced to our model of the ring. To keep our study within certain frames and to concentrate on the reflection symmetry issue, in this paper we confine ourselves to a description with the equivalent for electron and hole function $F_V(\mathbf{r})$. Therefore, in this study,

$$M(\mathbf{r}) = M_e(\mathbf{r}) = M_h(\mathbf{r}) = F_V(\mathbf{r})T(\mathbf{r}). \tag{14}$$

We present the position-dependent effective mass $m_{e\,(h)}(\mathbf{r})$ of electrons (holes), band gap $E_g(\mathbf{r})$, and dielectric constant $\epsilon(\mathbf{r})$ of the system as follows:

$$m_{e\,(h)}(\mathbf{r}) = m^{\text{in}}_{e\,(h)}M(\mathbf{r}) + m^{\text{out}}_{e\,(h)}[1 - M(\mathbf{r})], \tag{15}$$

$$E_g(\mathbf{r}) = E^{\text{in}}_g M(\mathbf{r}) + E^{\text{out}}_g[1 - M(\mathbf{r})], \tag{16}$$

$$\epsilon(\mathbf{r}) = \epsilon^{\text{in}} M(\mathbf{r}) + \epsilon^{\text{out}}[1 - M(\mathbf{r})]. \tag{17}$$

The Hamiltonian of the single neutral exciton within the effective position-dependent mass approximation reads[30,33,40,47]

$$\hat{H}_{\text{ext}} = \sum_{i=e,h} \hat{\mathbf{\Pi}}_i \frac{1}{2m_i(\mathbf{r}_i)} \hat{\mathbf{\Pi}}_i + \sum_{i=e,h} V_i(\mathbf{r}_i) + V_C(r_e,r_h), \tag{18}$$

where $\hat{\mathbf{\Pi}}_{e\,(h)} = -\hbar\nabla_{\mathbf{r}_{e\,(h)}} - q_{e\,(h)}\mathbf{A}(\mathbf{r}_{e(h)})$ is the electron (hole) momentum operator, $\nabla_{\mathbf{r}_{e\,(h)}}$ is the spatial gradient in the electron (hole) coordinate system, $q_{e\,(h)} = -(+)e$, and $\mathbf{A}(\mathbf{r})$ is the vector potential of the magnetic field, $\mathbf{B}(\mathbf{r}) = \nabla_{\mathbf{r}} \times \mathbf{A}(\mathbf{r})$. $V_C(\mathbf{r}_e,\mathbf{r}_h)$ presents the attractive electron-hole Coulomb interaction, which can be written as

$$V_C(\mathbf{r}_e,\mathbf{r}_h) = -e^2 G(\mathbf{r}_e,\mathbf{r}_h), \tag{19}$$

where $G(\mathbf{r}_e,\mathbf{r}_h)$ is the Green's function of the Poisson equation,[48,49]

$$\epsilon_0 \nabla_{\mathbf{r}} \epsilon(\mathbf{r}) \nabla_{\mathbf{r}} G(\mathbf{r},\mathbf{r}') = -\delta(\mathbf{r} - \mathbf{r}'). \tag{20}$$

For systems without reflection symmetry, the conventional Coulomb cylindrically symmetric gauge for the vector potential $\mathbf{A}(\mathbf{r})$ and uniform magnetic field $\mathbf{B}$ [$\mathbf{A}(\mathbf{r}) = \frac{1}{2}\mathbf{B} \times \mathbf{r}$] leads to unphysical behavior of the magnetic coupling part of the energy of a particle (see, for instance, Refs. 50–52 and references therein). This is an "origin-dependent gauge," which suggests at the very beginning that the expectation value of the position of a particle in the ground state ($\bar{\mathbf{r}}$) is exactly at the origin of the coordinate system ($\bar{\mathbf{r}} = \mathbf{0}$), which is not correct in general for the particle ground state in a system without reflection symmetry. For the results to be reliable, it is essential that the system model is rigorously invariant with respect to the gauge origin.[50–52] To satisfy this condition (according to the principle of the minimal magnetic coupling)[53–55] we use agauge-origin-independent definition for the vector potential:

$$\mathbf{A}(\mathbf{r}) = \tfrac{1}{2}\mathbf{B} \times (\mathbf{r} - \bar{\mathbf{r}}). \tag{21}$$

Using this gauge and Eq. (18) for the weak-field limit (when the magnetic field is applied along the z direction), we can write the exciton diamagnetic coefficient as

$$\alpha_d = \frac{e^2}{8}\left\langle \frac{(\boldsymbol{\rho}_e - \bar{\boldsymbol{\rho}}_e)^2}{m_e(\mathbf{r}_e)} + \frac{(\boldsymbol{\rho}_h - \bar{\boldsymbol{\rho}}_h)^2}{m_h(\mathbf{r}_h)} \right\rangle \Bigg|_{B=0}, \tag{22}$$

where $\boldsymbol{\rho} = (x,y)$ is the two-dimensional radius vector in the x-y plane, $\langle f \rangle$ stands for the expectation value of a quantity f in the exciton ground state,

$$\langle f \rangle = \int \Psi^*_G(\mathbf{r}_e,\mathbf{r}_h) f(\mathbf{r}_e,\mathbf{r}_h) \Psi_G(\mathbf{r}_e,\mathbf{r}_h) d\mathbf{r}_e d\mathbf{r}_h \tag{23}$$

[$\Psi_G(\mathbf{r}_e,\mathbf{r}_h)$ is the exciton ground-state wave function], and $\bar{\boldsymbol{\rho}}_{e\,(h)} = \langle \boldsymbol{\rho}_{e\,(h)} \rangle$ is the expectation value of the electron (hole) position in the x-y plane.

We use the Hartree approximation when the exciton wave function is presented by a product of the electron $\psi_e(\mathbf{r}_e)$ and hole $\psi_h(\mathbf{r}_h)$ wave functions: $\Psi_G(\mathbf{r}_e,\mathbf{r}_h) = \psi_e(\mathbf{r}_e)\psi_h(\mathbf{r}_h)$. The functions have to be obtained by solving self-consistently the following system of equations:[48]

$$[\hat{H}_e(\mathbf{r}_e) + V_h(\mathbf{r}_e)]\psi_e(\mathbf{r}_e) = E_e\psi_e(\mathbf{r}_e), \tag{24}$$

$$[\hat{H}_h(\mathbf{r}_h) + V_e(\mathbf{r}_h)]\psi_h(\mathbf{r}_h) = E_h\psi_h(\mathbf{r}_h), \tag{25}$$

TABLE I. Geometrical parameters of two types of rings.

Type	R (nm)	h_m (nm)	h_0 (nm)	h_∞ (nm)	ξ_h	ξ_R	ξ_γ
A	9	3.6	1.6	0.4	0.2	0.0	−0.25
B	7	2.1	1.0	0.4	0.15	0.07	0.0

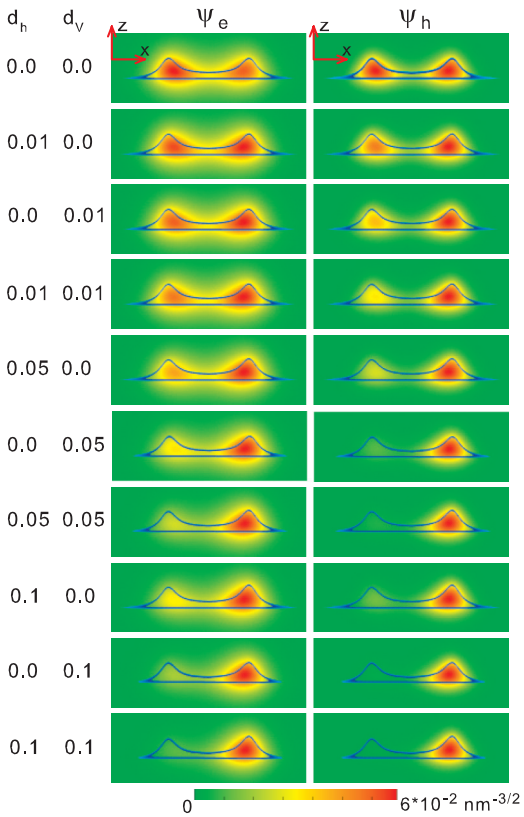

FIG. 4. (Color online) Contour plot of the ground-state wave function of the noninteracting electron and hole in the (x,y_p,z) plane for different positive values of the parameters d_h and d_V (type-A ring).

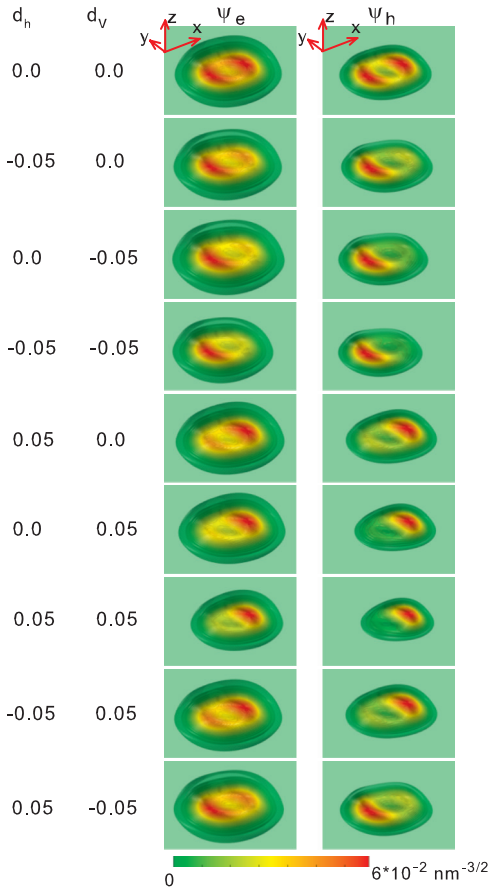

FIG. 5. (Color online) Three-dimensional contour plot of the ground-state wave function of the noninteracting electron and hole for different configurations of the type-A ring.

$$\epsilon_0 \nabla_{\mathbf{r}} \epsilon(\mathbf{r}) \nabla_{\mathbf{r}} V_{e(h)}(\mathbf{r}) = e^2 |\psi_{e(h)}(\mathbf{r})|^2, \tag{26}$$

where $\hat{H}_{e(h)}$ is the effective one-band Hamiltonian for the electron (hole) confined in the ring:

$$\hat{H}_{e(h)}(\mathbf{r}) = \hat{\mathbf{\Pi}}_{e(h)} \frac{1}{2m_{e(h)}(\mathbf{r})} \hat{\mathbf{\Pi}}_{e(h)} + V_{e(h)}(\mathbf{r}). \tag{27}$$

The exciton ground-state energy in this approximation is defined as

$$E_{\text{ext}} = E_g^{\text{in}} + E_e + E_h - \frac{1}{2}\left[\int |\psi_e(\mathbf{r})|^2 V_h(\mathbf{r}) d\mathbf{r} + \int |\psi_h(\mathbf{r})|^2 V_e(\mathbf{r}) d\mathbf{r}\right]. \tag{28}$$

III. SIMULATION RESULTS AND DISCUSSION

We compute the exciton ground-state wave function, energy, and diamagnetic coefficient for two types of asymmetrical $In_cAs_{1-c}Ga/GaAs$ SAQRs: A and B. Geometrical parameters of the type-A ring are close to those of the rings discussed in Refs. 13, 37, and 39, and the parameters for the type-B ring are chosen according to the data from Ref. 38. Table I presents basic geometrical parameters for both types of rings. Other relevant geometrical parameters are taken as $x_p = R(1+\xi_R)$, $y_p = 0$, $z_p = 0.6h_m$, $b = x_p$, $b_z = h_m$, $a = 0.4$ nm, and $\gamma_0 = \gamma_\infty = 3$ nm. In Fig. 1, we show (for the type-A ring with and without the reflection symmetry) the ring's height profiles along the x axis $[h(x,0)]$ and along a direction which is parallel to the y axis $[h(x_p,y)]$. Material parameters for $In_cAs_{1-c}Ga/GaAs$ heterostructures we take from Refs. 48 and 56 and adjust them according to the actual composition and strain inside the rings:[43,49,57] $E_{g\text{InAs}} = 0.842$ eV, $m_{e\text{InAs}} = 0.044m_0$, $m_{h\text{InAs}} = 0.074m_0$, $\epsilon_{\text{InAs}} = 15.1$, $E_{g\text{GaAs}} = 1.52$ eV, $m_{e\text{GaAs}} = 0.067m_0$, $m_{h\text{GaAs}} = 0.5m_0$, $\epsilon_{\text{GaAs}} = 12.9$ (m_0 is the free-electron mass). A material parameter $D^{\text{in (out)}}$ for the $In_cGa_{1-c}As$ compound is obtained according to the linear interpolation $D_c = cD_{\text{InAs}} + (1-c)D_{\text{GaAs}}$. The In concentration inside rings is taken to be $c = 0.55$ and 0.7 for types A and B, respectively. In addition, we take 70% of the heterostructure gap difference to be the conductance band offset and 30% to be the valence band offset in the rings. The energy and wave function of the exciton confined in the SAQRs are obtained numerically form the self-consistent solution of Eqs. (24)–(26) by the iterative method using the COMSOL MULTIPHYSICS package.[58] We use the wave function to simulate the exciton diamagnetic coefficient [Eq. (22)] for SAQRs with the reflection symmetry and when the symmetry is broken.

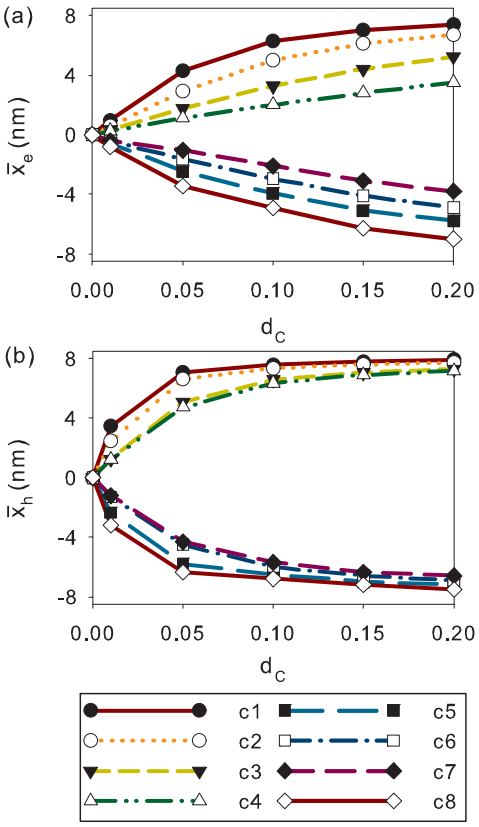

FIG. 6. (Color online) The expectation value of the position of the noninteracting electron (a) and hole (b) in the ground state on the x axis (type-A ring). The parameter d_C represents simultaneous changes of d_h and d_V for different configurations: (c1) $d_C = d_h = d_V \geqslant 0$; (c2) $d_h = 0, d_C = d_V \geqslant 0$; (c3) $d_C = d_h \geqslant 0, d_V = 0$; (c4) $d_C = |d_h| = d_V, d_h \leqslant 0, d_V \geqslant 0$; (c5) $d_h = 0, d_C = |d_V|; d_V \leqslant 0$; (c6) $d_C = |d_h|; d_h \leqslant 0, d_V = 0$; (c7) $d_C = d_h = |d_V|, d_h \geqslant 0, d_V \leqslant 0$; (c8) $d_C = |d_h| = |d_V|, d_h \leqslant 0, d_V \leqslant 0$.

First we present the ground-state wave functions of the noninteracting electron and hole for the type-A ring at zero magnetic field. We independently consider the impacts of the ring's shape reflection asymmetry and content reflection asymmetry on the electron and hole wave functions inside the ring. In Fig. 4, we show the contour plot of the x-y plane cross section of the electron and hole ground-state wave functions. When two parameters d_h and d_V change from 0 (reflectional symmetrical ring) to 0.1, the wave functions change from a reflectional symmetrical ringlike function (extended around the ring volume) to reflection nonsymmetrical quantum dotlike wave functions (localized in one of the potential valleys of the ring near $x = x_p$). Note that the wave functions are localized in one of the potential valleys when the imbalance in the ring potential profile is relatively small. Both the electron and hole wave functions are more sensitive to the variations of the parameter d_V. At the same time, the hole wave function is generally more sensitive to the imbalance in the reflection symmetry, which can be understood as a consequence of the particles' effective-mass difference: as the hole has a larger effective mass, the effect of the imbalance is stronger.

Figure 5 shows that for negative values of the parameters d_h and d_V, the electron and hole wave function mean localization positions move in the direction of $x = -x_p$. However, for the cases in which the parameters have different signs ("anticorrelation"), the position of the localization is controlled by the sign of d_V. Notice that the change of the parameters' signs in our description does not generate a simple symmetrical reflection in the y-z plane for the wave functions (compare, for instance, the cases $\{d_h = 0.05, d_V = 0.05\}$ and $\{d_h = -0.05, d_V = -0.05\}$). This can be understood from Figs. 1 and 2. It is clear that the transformations $d_h \Rightarrow -d_h$ and $d_V \Rightarrow -d_V$ cannot be presented as $\mathbf{C}_2$ rotations of the ring.

For a better understanding of the impact of the broken reflection symmetry in the wobbled rings on the actual localization positions and characteristic confinement lengths of the electron and hole, we study the expectation value of the ground-state electron (hole) position $\bar{\boldsymbol{\rho}}_{e(h)} = (\bar{x}_{e(h)}, \bar{y}_{e(h)})$ in the x-y plane and the mean (effective) lateral electron (hole) radius

$$\rho_{e(h)} = \sqrt{\langle(\boldsymbol{\rho}_{e(h)} - \bar{\boldsymbol{\rho}}_{e(h)})^2\rangle}$$

for the type-A ring at zero magnetic field. For all configurations, the expectation value of the electron (hole) position on the y axes remains unchanged: $\bar{y}_{e(h)} = 0$. Figure 6 shows $\bar{x}_{e(h)}$ of the noninteracting electron and hole in the ground states for different values and combinations of d_h and d_V. When the absolute values of the parameters d_h and d_V increase, the electron mean position gradually moves from the center of the ring toward one (appropriate) of the unbalanced potential valleys. At the same time, the hole mean position is almost stabilized in the valley when parameters d_h or d_V are only

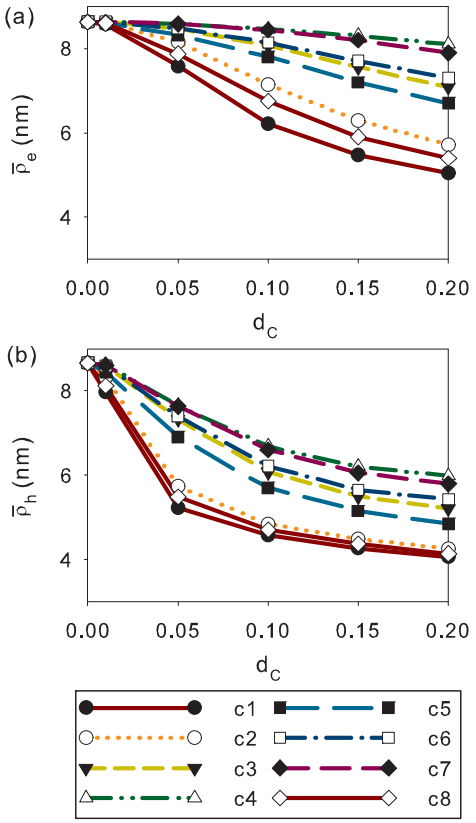

FIG. 7. (Color online) The effective lateral radius of the noninteracting electron (a) and hole (b) (type-A ring). The configurations c1, . . . ,c8 are described in the caption to Fig. 6.

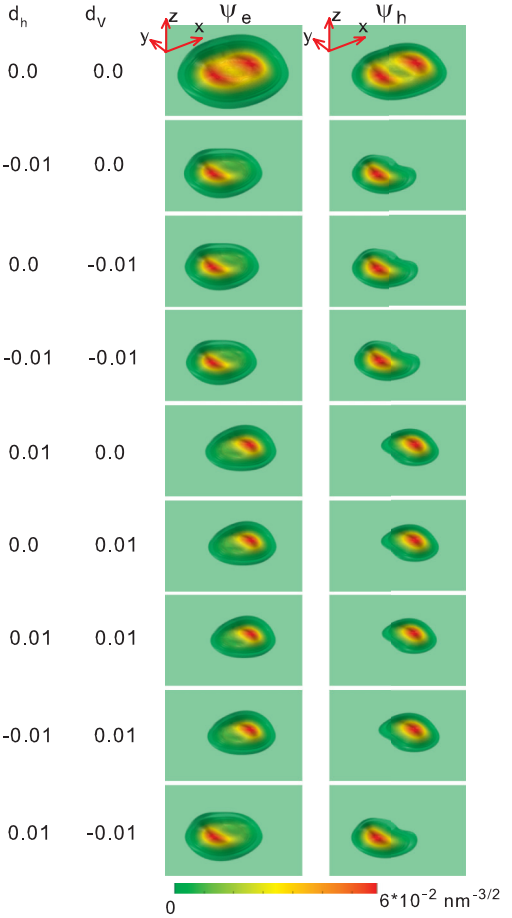

FIG. 8. (Color online) Three-dimensional contour plot of the electron and hole components of the exciton ground-state wave function for different configurations of the type-A ring.

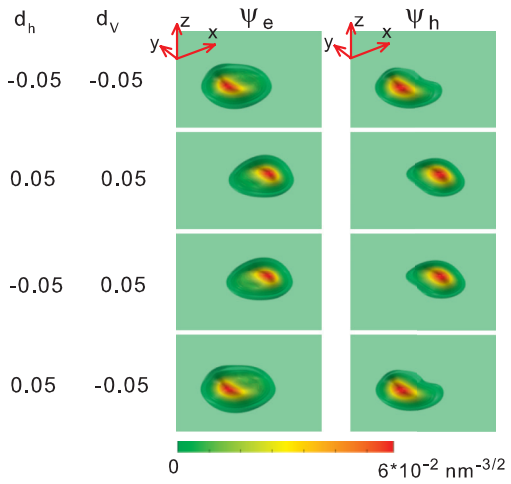

FIG. 9. (Color online) Three-dimensional contour plot of the electron and hole component of the exciton ground-state wave function for different configurations of the type-A ring for $d_C = |d_h| = |d_V| = 0.05$ (see Fig. 6).

about 0.1 in the absolute value. Furthermore, from Fig. 7 we see that the effective lateral radii of the electron and hole follow the same tendency: the electron's radius decreases smoothly and the hole's radius shrinks rapidly.

The interparticle interaction drastically changes the sensitivity of the particles' wave functions to the imbalance in

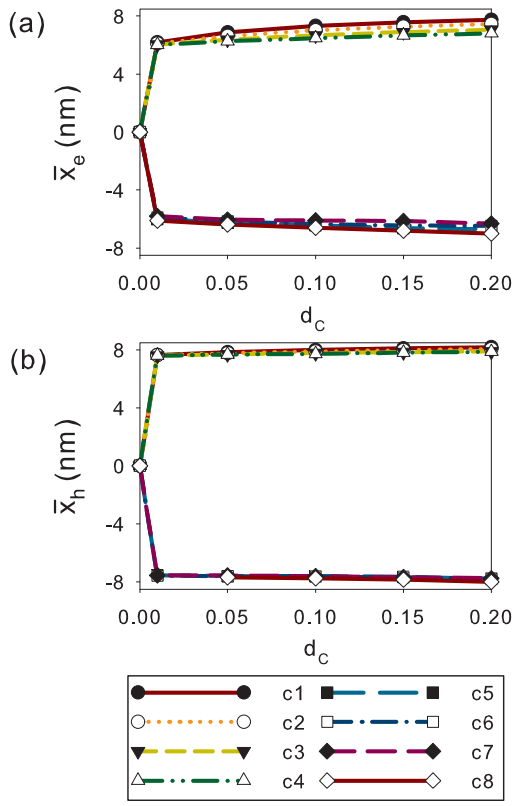

FIG. 10. (Color online) The expectation value of the position of the electron (a) and hole (b) on the x axis for the exciton in the ground state (type-A ring). The configurations c1, . . . ,c8 are described in the caption to Fig. 6.

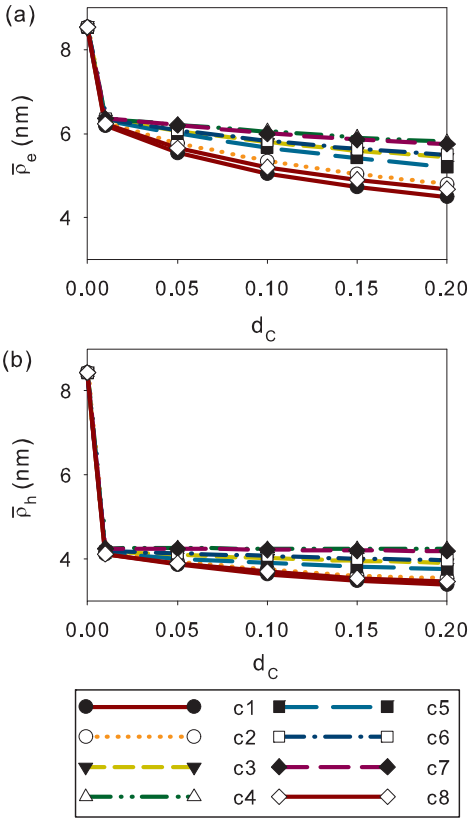

FIG. 11. (Color online) The effective lateral radius of the electron (a) and hole (b) for the exciton in the ground state (type-A ring). The configurations c1, . . . ,c8 are described in the caption to Fig. 6.

the reflection symmetry of the ring. We show in Fig. 8 the electron and hole components of the ground-state exciton wave function [self-consistent solutions of Eqs. (24)–(26)]. Now even very small (∼0.01) nonzero d_h and (or) d_V generate the simultaneous localization of the electron and hole wave functions (the ground-state exciton wave function) in one of the potential valleys. The reason is that the Coulomb interaction makes the electron and hole move in the same direction of the position of the hole (dotlike wave function). The actual mean position $\bar{x}_{e(h)}$ is controlled by the sign of d_V. Figure 9 shows that a further increase of d_h and d_V magnitudes does not considerably affect the wave functions which are well localized in one of the potential valleys.

The high sensitivity of the holes to the imbalance in the reflection symmetry of the ring is a "triggering factor" in the "one-valley localization effect" for the exciton. We demonstrate in Fig. 10 that the dependency of the electron mean localization position on d_h and d_V becomes very similar to that for the hole when we impose the electron-hole interaction. Moreover, the Coulomb interaction makes the electron and hole effective lateral radii both very sensitive to the reflection asymmetry of the ring: the radii simultaneously and rapidly decrease when a small imbalance appears, as is shown in Fig. 11 (compare with Fig. 7).

With the obtained actual positions of the electron and hole components of the ground-state exciton wave function, we examine now the effect of the reflectional asymmetry on the exciton diamagnetic coefficient α_d [Eq. (22)]. In

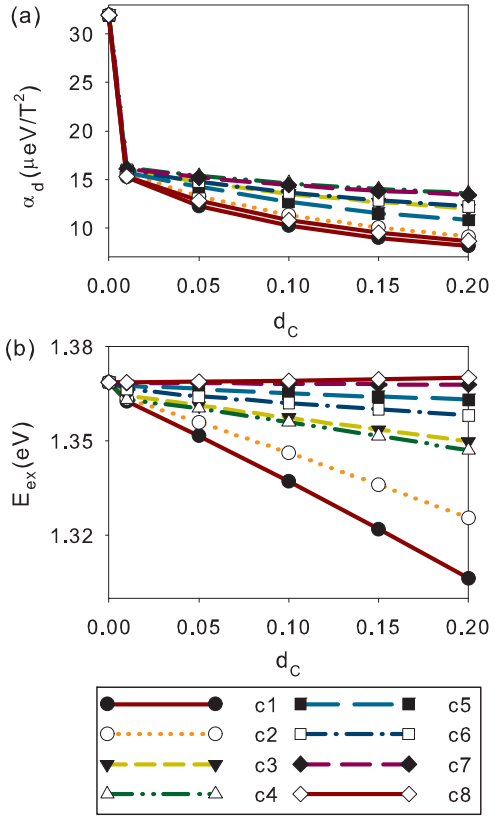

FIG. 12. (Color online) Exciton diamagnetic coefficient (a) and ground-state energy (b) for the type-A ring. The configurations c1, . . . ,c8 are described in the caption to Fig. 6.

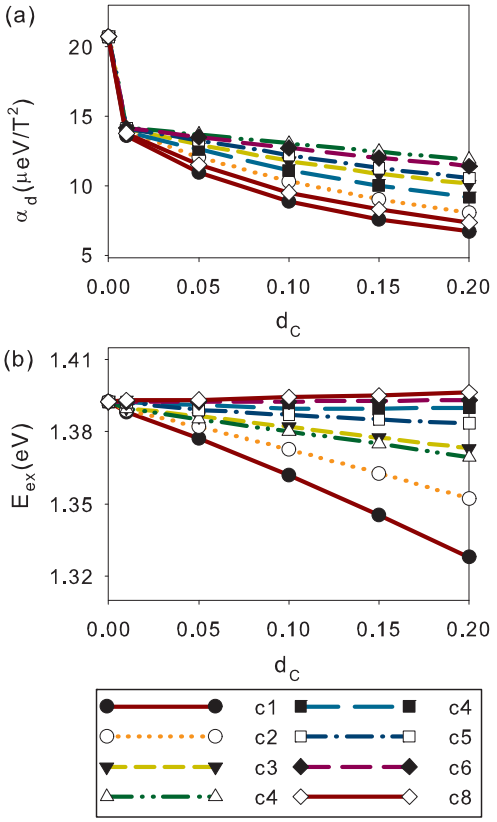

FIG. 13. (Color online) Exciton diamagnetic coefficient (a) and ground-state energy (b) for the type-B ring. The configurations c1, . . . ,c8 are described in the caption to Fig. 6.

Fig. 12(a), we show the dependence of the exciton diamagnetic coefficient on the parameters d_h and d_V. It is clear that the above-described sensitivity of the electron and hole wave functions' localizations and distributions to the imbalance in the reflection symmetry leads to a rapid decrease of the exciton diamagnetic coefficient (about two times) already for small values of d_h and d_V (about 0.01 in magnitude). However, the coefficient decreases only gradually when the ring's geometry and material content become more unbalanced along the x direction.

Figure 12(b) shows our simulation results for the ground-state energy of the exciton confined in the ring. Clearly, according to the actual profiles of the energy gap and confinement potential in the structure (see Fig. 3), the exciton energy can decrease, increase, and remain unchanged when the absolute values of the parameters d_h and d_V increase. Notice that the positive nonzero d_V always leads to an effective decrease of the distance between the bottom of the conduction band and the top of the valence band [$E_g(\mathbf{r}_p)$], which causes the exciton energy to decrease when d_V is growing. When the parameter d_V is taken to be negative and (or) we impose $d_h \neq 0$, the effective band gap (the smallest distance between the bottom of the conduction band and the top of the valence band) does not change. Some minor growth of the self-consistent energies of the electron and hole (because of their dotlike confinement in one of the valleys) is mainly compensated by an increase of the electron-hole Coulomb interaction. As a result of those factors' combination, the exciton energy can decrease slightly, increase, or even remain unchanged for $d_V < 0$ [see Fig. 12(b)].

Let us now consider the quantum ring of the type B. The impact of the broken reflection symmetry on the characteristics of this ring is similar to that for the type-A ring (see Fig. 13). The mean localization positions and effective radii of the noninteracting and interacting electron and hole follow the general dependencies described above for the type-A ring. Nevertheless, the rim radius of the type-B ring is smaller than that for the type-A ring (see Table I). This obviously leads to a smaller value of the exciton diamagnetic coefficient for the reflection symmetrical ring ($d_h = d_V = 0$). When the symmetry is broken, the exciton diamagnetic coefficient decreases rapidly and it remains gradually decreasing when the absolute values of the parameters d_h and d_V increase up to 0.2 [Fig. 13(a)]. Note that in the type-B ring, the distance between potential valleys is smaller than that in the type-A ring. Therefore, even when the exciton wave function is mainly localized in one of the potential valleys, the small distance between the valleys causes some "relict" penetration of the function into the opposite valley. By increasing the absolute values of the parameters d_h and d_V, the electron and hole wave functions gradually shrink near the mean localization position. This results in the gradual decrease of the exciton diamagnetic coefficient, which is more visible than that for the type-A ring. In Fig. 13(b), we show the ground-state exciton energy for the type-B ring. Comparing with Fig. 12(b), we notice that

the dependence of the energy on the parameters d_h and d_V in general has the same explanation as for the type-A ring.

Our results for both types of rings agree well with experimental data.[13,38] Furthermore, by comparing Figs. 12(a) and 13(a) with the data from Refs. 13, 38, and 39, we can suggest that for the type-A ring, the reflection asymmetry can be characterized by $|d_h| \simeq |d_V| \approx 0.1$ ($\alpha_d \approx 10\ \mu\text{eV/T}^2$), while for the type-$B$ ring it can be characterized by $|d_h| \simeq |d_V| \approx 0.2$ ($\alpha_d \approx 7\mu\text{eV/T}^2$). This is consistent with our results for the exciton ground-state energy. The best agreement we obtain with the experimental data for the exciton energy is when the parameters d_h and d_V are chosen to be in between $+0.1$ and $+0.15$ (type-A ring), and in between $+0.15$ and $+0.2$ (type-B ring). Notice that for both types of quantum rings, our results suggest a strong "correlation" between d_h and d_V.

IV. CONCLUSION

In this paper, using the mapping method and Hartree approximation, we calculated the diamagnetic coefficient for the neutral exciton confined in $\text{In}_c\text{As}_{1-c}\text{Ga/GaAs}$ wobbled SAQRs. We have systematically investigated the impact of the rings' reflection asymmetry on the exciton ground-state wave function localization, energy, and diamagnetic coefficient. Two types of the rings known from experimental works were considered. Deviations from the reflection symmetry caused by the imperfect ring shape and material content are controlled by the parameters d_h and d_V, respectively (the case $d_h = d_V = 0$ stands for the reflection symmetrical ring). We have found that for the noninteracting particles, the electron wave function is more stable to the unbalance in the ring reflection symmetry than the hole wave function. This originates from the difference in the particles' effective masses. The Coulomb interaction causes the localization of the exciton wave function in one of the potential valleys of the wobbled ring for very small deviations of the parameters d_h and d_V from zero. Moreover, the effective lateral radii of the electron and hole are shrinking rapidly when the absolute values of the parameters d_h and d_V are growing. This results in the rapid decrease of the neutral exciton diamagnetic coefficient. After the rapid drop, the diamagnetic coefficient only gradually decreases with the further increase of the magnitudes of parameters d_h and d_V. In addition, we have found that a "correlative" imbalance in the ring geometry and material content has a recognizable impact on the ground-state energy of the neutral exciton. Our results are in good agreement with experimental observations. Moreover, they can give a very useful insight into the actual magneto-optical properties of the self-assembled semiconductor quantum rings. We note that a strong sensitivity of the magneto-optical properties to the actual imbalance in the reflection symmetry (which is very likable in experiments) and the rapid transition from the ringlike exciton wave function to the dotlike exciton wave function can be a reason for the optical Aharonov-Bohm effect suppression in $\text{In}_c\text{As}_{1-c}\text{Ga/GaAs}$ wobbled rings. At the same time, the wave function of an independent election is less sensitive to the lack of the reflection symmetry, which helps to explain the observation of the Aharonov-Bohm magnetization oscillation even in quantum rings with broken reflection symmetry.

More generally, our approach can be used for the realistic modeling of the magneto and magneto-optical characteristics of semiconductor nano-objects with realistic and nonsymmetrical geometry and material content.

ACKNOWLEDGMENTS

This work is supported by the National Science Council of the Republic of China under Contracts No. NSC 101-3113-P-009-004 and No. NSC 101-2112-M-009-010, and Aiming for the Top University Program of the National Chiao Tung University.

*Author to whom all correspondence should be addressed: vam@faculty.nctu.edu.tw

[1] J. M. García, G. Medeiros-Ribeiro, K. Schmidt, T. Ngo, J. L. Feng, A. Lorke, J. Kotthaus, and P. M. Petroff, Appl. Phys. Lett. **71**, 2014 (1997).
[2] A. Lorke and R. J. Luyken, Physica B **256–258**, 424 (1998).
[3] A. Lorke, R. J. Luyken, A. O. Govorov, J. P. Kotthaus, J. M. García, and P. M. Petroff, Phys. Rev. Lett. **84**, 2223 (2000).
[4] A. Fuhrer, S. Lüscher, T. Ihn, T. Heinzel, K. Ensslin, W. Wegscheider, and M. Bichler, Nature (London) **413**, 822 (2001).
[5] B. C. Lee, O. Voskoboynikov, and C. P. Lee, Physica E **24**, 87 (2004).
[6] Y. Aharonov and D. Bohm, Phys. Rev. **115**, 485 (1959).
[7] A. V. Chaplik, JETP **92**, 169 (2000).
[8] D. Haft, C. Schulhauser, A. O. Govorov, R. J. Warburton, K. Karraia, J. M. Garcia, W. Schoenfeld, and P. M. Petroff, Physica E **13**, 165 (2002).
[9] A. O. Govorov, A. V. Kalameitsev, R. Warburton, K. Karrai, and S. E. Ulloa, Physica E **13**, 297 (2002).
[10] A. O. Govorov, S. E. Ulloa, K. Karrai, and R. J. Warburton, Phys. Rev. B **66**, 081309 (2002).
[11] M. Bayer, M. Korkusinski, P. Hawrylak, T. Gutbrod, M. Michel, and A. Forchel, Phys. Rev. Lett. **90**, 186801 (2003).
[12] L. G. G. V. Dias da Silva, S. E. Ulloa, and T. V. Shahbazyan, Phys. Rev. B **72**, 125327 (2005).
[13] N. A. J. M. Kleemans, J. H. Blokland, A. G. Taboada, H. C. M. van Genuchten, M. Bozkurt, V. M. Fomin, V. N. Gladilin, D. Granados, J. M. García, P. C. M. Christianen, J. C. Maan, J. T. Devreese, and P. M. Koenraad, Phys. Rev. B **80**, 155318 (2009).
[14] M. D. Teodoro, V. L. Campo, V. Lopez-Richard, E. Marega, G. E. Marques, Y. G. Gobato, F. Iikawa, M. J. S. P. Brasil, Z. Y. AbuWaar, V. G. Dorogan, Y. I. Mazur, M. Benamara, and G. J. Salamo, Phys. Rev. Lett. **104**, 086401 (2010).
[15] F. Ding, N. Akopian, B. Li, U. Perinetti, A. Govorov, F. M. Peeters, C. C. Bof Bufon, C. Deneke, Y. H. Chen, A. Rastelli, O. G. Schmidt, and V. Zwiller, Phys. Rev. B **82**, 075309 (2010).
[16] J. Cui, Q. He, X. M. Jiang, Y. L. Fan, X. J. Yang, F. Xue, and Z. M. Jiang, Appl. Phys. Lett. **83**, 2907 (2003).

[17]P. Offermans, P. M. Koenraad, J. H. Wolter, D. Granados, J. M. García, V. M. Fomin, V. N. Gladilin, and J. T. Devreese, Appl. Phys. Lett. **87**, 131902 (2005).
[18]T. Mano, T. Kuroda, S. Sanguinetti, T. Ochiai, T. Tateno, J. Kim, T. Noda, M. Kawabe, K. Sakoda, G. Kido, and N. Koguchi, Nano Lett. **5**, 425 (2005).
[19]T. Kuroda, T. Mano, T. Ochiai, S. Sanguinetti, K. Sakoda, G. Kido, and N. Koguchi, Phys. Rev. B **72**, 205301 (2005).
[20]J. Sormunen, J. Riikonen, M. Mattila, J. Tiilikainen, M. Sopanen, and H. Lipsanen, Nano Lett. **5**, 1541 (2005).
[21]S. Huang, Z. Niu, Z. Fang, H. Ni, Z. Gong, and J. Xia, Appl. Phys. Lett. **89**, 031921 (2006).
[22]F. Ding, L. Wang, S. Kiravittaya, E. Müller, A. Rastelli, and O. G. Schmidt, Appl. Phys. Lett. **90**, 173104 (2007).
[23]R. Timm, A. Lenz, H. Eisele, L. Ivanova, M. Dähne, G. Balakrishnan, D. L. Huffaker, I. Farrer and D. A. Ritchie, J. Vac. Sci. Technol. B **26**, 1492 (2008).
[24]C. Somaschini, S. Bietti, N. Koguchi, and S. Sanguinetti, Nano Lett. **9**, 3419 (2009).
[25]C.-H. Lee, C. W. Liu, H.-T. Chang, and S. W. Lee, J. Appl. Phys. **107**, 056103 (2010).
[26]P. Moon, W. J. Choi, K. Park, E. Yoon, and J. Lee, J. Appl. Phys. **109**, 103701 (2011).
[27]G. Cohen-Taguri, A. Ruzin, and I. Goldfar, Appl. Phys. Lett. **100**, 213116 (2012).
[28]M. D. Teodoro, A. Malachias, V. Lopes-Oliveira, D. F. Cesar, V. Lopez-Richard, G. E. Marques, E. Marega, Jr., M. Benamara, Yu. I. Mazur, and G. J. Salamo, J. Appl. Phys. **112**, 014319 (2012).
[29]J. Planelles, W. Jaskólski, and J. I. Aliaga, Phys. Rev. B **65**, 033306 (2001).
[30]O. Voskoboynikov, Y. Li, H.-M. Lu, C. -F. Shih, and C. P. Lee, Phys. Rev. B **66**, 155306 (2002).
[31]J. I. Climente, J. Planelles, and W. Jaskolski, Phys. Rev. B **68**, 075307 (2003).
[32]J. A. Barker, R. J. Warburton, and E. P. O'Reilly, Phys. Rev. B **69**, 035327 (2004).
[33]J. I. Climente, J. Planelles, and J. L. Movilla, Phys. Rev. B **70**, 081301 (2004).
[34]P. Offermans, P. M. Koenraad, J. H. Wolter, D. Granados, J. M. García, V. M. Fomin, V. N. Gladilin, and J. T. Devreese, Physica E **32**, 41 (2006).
[35]N. A. J. M. Kleemans, I. M. A. Bominaar-Silkens, V. M. Fomin, V. N. Gladilin, D. Granados, A. G. Taboada, J. M. García, P. Offermans, U. Zeitler, P. C. M. Christianen, J. C. Maan, J. T. Devreese, and P. M. Koenraad, Phys. Rev. Lett. **99**, 146808 (2007).
[36]V. M. Fomin, V. N. Gladilin, S. N. Klimin, J. T. Devreese, N. A. J. M. Kleemans, and P. M. Koenraad, Phys. Rev. B **76**, 235320 (2007).
[37]V. M. Fomin, V. N. Gladilin, J. T. Devreese, N. A. J. M. Kleemans, M. Bozkurt, and P. M. Koenraad, Phys. Status Solidi B **245**, 2657 (2008).
[38]T.-C. Lin, C.-H. Lin, H.-S. Ling, Y.-J. Fu, W.-H. Chang, S.-D. Lin, and C.-P. Lee, Phys. Rev. B **80**, 081304(R) (2009).
[39]V. M. Fomin, V. N. Gladilin, J. T. Devreese, J. H. Blokland, P. C. M. Christianen, J. C. Maan, A. G. Taboada, D. Granados, J. M. García, N. A. J. M. Kleemans, H. C. M. van Genuchten, M. Bozkurt, and P. M. Koenraad, Proc. SPIE **7364**, 736402 (2009).
[40]B. Li and F. M. Peeters, Phys. Rev. B **83**, 115448 (2011).
[41]F. Ding, B. Li, N. Akopian, U. Perinetti, Y. H. Chen, F. M. Peeters, A. Rastelli, V. Zwiller, and O. G. Schmidt, J. Nanoelectron. Optoelectron. **6**, 51 (2011).
[42]M. Tadić, N. Ćukarić, V. Arsoski, and F. M. Peeters, Phys. Rev. B **84**, 125307 (2011).
[43]L. M. Thu, W. T. Chiu, and O. Voskoboynikov, Phys. Rev. B **85**, 205419 (2012).
[44]S. N. Walck and T. L. Reinecke, Phys. Rev. B **57**, 9088 (1998).
[45]L. D. Landau and E. M. Lifshitz, *Quantum Mechanics: Non-relativistic Theory* (Pergamon, New York, 1977).
[46]L. M. Thu, W. T. Chiu, and O. Voskoboynikov, Phys. Rev. B **83**, 125301 (2011).
[47]G. Bastard, *Wave Mechanics Applied to Semiconductor Heterostructures* (Les Edition de Physique, Les Ulis, France, 1990).
[48]O. Stier, M. Grundmann, and D. Bimberg, Phys. Rev. B **59**, 5688 (1999).
[49]L. M. Thu and O. Voskoboynikov, Phys. Rev. B **80**, 155442 (2009).
[50]S. Pelloni, P. Lazzeretti, and R. Zanasi, J. Phys. Chem. A **113**, 14465 (2009).
[51]K. K. Lange, E. I. Tellgren, M. R. Hoffmann, and T. Helgaker, Science **337**, 327 (2012).
[52]T. Helgaker, S. Coriani, P. Jørgensen, K. Kristensen, J. Olsen, and K. Ruud, Chem. Rev. **112**, 543 (2012).
[53]T. K. Rebane, Zh. Eksp. Teor. Fiz. **38**, 963 (1960) [Sov. Phys. JETP **11**, 694 (1960)].
[54]O. E. Raichev and F. T. Vasko, Phys. Rev. B **53**, 1522 (1996).
[55]A. I. Ivanov and O. R. Lobanova, Physica E **23**, 61 (2004).
[56]I. Vurgaftman, J. R. Meyer, and L. R. Ram-Mohan, J. Appl. Phys. **89**, 5815 (2001).
[57]C. E. Pryor and M.-E. Pistol, Phys. Rev. B **72**, 205311 (2005).
[58]www.comsol.com.